Citation for published version:

Gregory J. Herczeg, et al, 'How Do Stars Gain Their Mass? A JCMT/SCUBA-2 Transient Survey of Protostars in Nearby Star-forming Regions', *The Astrophysical Journal,* Vol. 849 (43), October 2017.

DOI:

Document Version:

This is the Accepted Manuscript version.
The version in the University of Hertfordshire Research Archive may differ from the final published version.

Copyright and Reuse:

Enquiries

If you believe this document infringes copyright, please contact the Research & Scholarly Communications Team at rsc@herts.ac.uk

HOW DO STARS GAIN THEIR MASS? A JCMT/SCUBA-2 TRANSIENT SURVEY OF PROTOSTARS IN NEARBY STAR FORMING REGIONS

Gregory J. Herczeg[1], Doug Johnstone[2,3], Steve Mairs[2,3], Jennifer Hatchell[4], Jeong-Eun Lee[5], Geoffrey C. Bower[6], Huei-Ru Vivien Chen[7], Yuri Aikawa[8], Hyunju Yoo[9,5], Sung-Ju Kang[10], Miju Kang[10], Wen-Ping Chen[11], Jonathan P. Williams[12], Jaehan Bae[13], Michael M. Dunham[14,15], Eduard I. Vorobiov[16,17,18], Zhaohuan Zhu[19], Ramprasad Rao[20], Helen Kirk[2], Satoko Takahashi[21,22], Oscar Morata[20], Kevin Lacaille[23], James Lane[3], Andy Pon[24], Aleks Scholz[25], Manash R. Samal[11], Graham S. Bell[26], Sarah Graves[26], E'lisa M. Lee[26], Harriet Parsons[26], Yuxin He[27], Jianjun Zhou[27], Mi-Ryang Kim[28], Scott Chapman[23], Emily Drabek-Maunder[29], Eun Jung Chung[10], Stewart P. S. Eyres[30], Jan Forbrich[31,15], Lynne A. Hillenbrand[32], Shu-ichiro Inutsuka[33], Gwanjeong Kim[10], Kyoung Hee Kim[34], Yi-Jehng Kuan[35,20], Woojin Kwon[10,36], Shih-Ping Lai[7,20], Bhavana Lalchand[11], Chang Won Lee[10,36], Chin-Fei Lee[20] Feng Long[1,37], A-Ran Lyo[10], Lei Qian[38], Peter Scicluna[20], Archana Soam[10], Dimitris Stamatellos[30], Shigehisa Takakuwa[39], Ya-Wen Tang[20], Hongchi Wang[40], Yiren Wang[1,37]

Draft version September 8, 2017

ABSTRACT

Most protostars have luminosities that are fainter than expected from steady accretion over the protostellar lifetime. The solution to this problem may lie in episodic mass accretion – prolonged periods of very low accretion punctuated by short bursts of rapid accretion. However, the timescale and amplitude for variability at the protostellar phase is almost entirely unconstrained. In *A JCMT/SCUBA-2 Transient Survey of Protostars in Nearby Star Forming Regions*, we are monitoring monthly with SCUBA-2 the sub-mm emission in eight fields within nearby (< 500 pc) star forming regions to measure the accretion variability of protostars. The total survey area of ~ 1.6 sq.deg. includes ~ 105 peaks with peaks brighter than 0.5 Jy/beam (43 associated with embedded protostars or disks) and 237 peaks of 0.125–0.5 Jy/beam (50 with embedded protostars or disks). Each field has enough bright peaks for flux calibration relative to other peaks in the same field, which improves upon the nominal flux calibration uncertainties of sub-mm observations to reach a precision of $\sim 2 - 3\%$ rms, and also provides quantified confidence in any measured variability. The timescales and amplitudes of any sub-mm variation will then be converted into variations in accretion rate and subsequently used to infer the physical causes of the variability. This survey is the first dedicated survey for sub-mm variability and complements other transient surveys at optical and near-IR wavelengths, which are not sensitive to accretion variability of deeply embedded protostars.

Subject headings: stars: protostars — stars: formation — submillimeter: general – circumstellar matter

[1] Kavli Institute for Astronomy and Astrophysics, Peking University, Yiheyuan 5, Haidian Qu, 100871 Beijing, People's Republic of China

[2] NRC Herzberg Astronomy and Astrophysics, 5071 West Saanich Rd, Victoria, BC, V9E 2E7, Canada

[3] Department of Physics and Astronomy, University of Victoria, Victoria, BC, V8P 5C2, Canada

[4] Physics and Astronomy, University of Exeter, Stocker Road, Exeter EX4 4QL, UK

[5] School of Space Research, Kyung Hee University, 1732, Deogyeong-Daero, Giheung-gu Yongin-shi, Gyunggi-do 17104, Korea

[6] Academia Sinica Institute of Astronomy and Astrophysics, 645 N. A'ohoku Place, Hilo, HI 96720, USA

[7] Department of Physics and Institute of Astronomy, National Tsing Hua University, Taiwan

[8] Department of Astronomy, University of Tokyo, Tokyo, Japan

[9] Chungnam National University, Korea

[10] Korea Astronomy and Space Science Institute, 776 Daedeokdae-ro, Yuseong-gu, Daejeon 34055, Republic of Korea

[11] Graduate Institute of Astronomy, National Central University, 300 Jhongda Road, Zhongli, Taoyuan, Taiwan

[12] Institute for Astronomy, University of Hawaii at Manoa, Honolulu, HI 96822, USA

[13] Department of Astronomy, University of Michigan, 1085 S. University Ave., Ann Arbor, MI 48109, USA

[14] Department of Physics, The State University of New York at Fredonia, Fredonia, NY 14063, USA

[15] Harvard-Smithsonian Center for Astrophysics, 60 Garden Street, Cambridge, MA 02138, USA

[16] Institute of Fluid Mechanics and Heat Transfer, TU Wien, Vienna, 1060, Austria

[17] Research Institute of Physics, Southern Federal University, Stachki Ave. 194, Rostov-on-Don, 344090, Russia

[18] University of Vienna, Department of Astrophysics, Vienna, 1180, Austria

[19] Physics and Astronomy Department, University of Nevada, Las Vegas

[20] Academia Sinica Institute of Astronomy and Astrophysics, P. O. Box 23-141, Taipei 10617, Taiwan

[21] Joint ALMA Observatory, Alonso de Córdova 3107, Vitacura, Santiago, Chile

[22] National Astronomical Observatory of Japa, 2-21-1 Osawa, Mitaka, Tokyo 181-8588, Japan

[23] Department of Physics and Atmospheric Science, Dalhousie University, Halifax, NS, B3H 4R2, Canada

[24] Department of Physics and Astronomy, The University of Western Ontario, 1151 Richmond Street, London, N6A 3K7, Canada

[25] SUPA, School of Physics & Astronomy, North Haugh, St Andrews, KY16 9SS, United Kingdom

[26] East Asian Observatory, 660 N. A'ohōkū Place, Hilo, HI 96720, USA

[27] Xinjiang Astronomical Observatory, Chinese Academy of Sciences, Urumqi, China

[28] Department of Physics, Institute for Astrophysics, Chungbuk National University, Republic of Korea

[29] Cardiff University, School of Physics and Astronomy, The Parade, Cardiff, CF24 3AA

[30] Jeremiah Horrocks Institute for Mathematics, Physics &

1. INTRODUCTION

Low-mass stars form through the gravitational collapse of molecular cloud cores. The evolution of mass accretion onto a forming protostar depends on the rate at which the interior of the core collapses, the role of the circumstellar disk as a temporary mass reservoir and transportation mechanism, and the physics of how the inner disk accretes onto the stellar surface. In dynamical models of gravitational collapse of a spherical protostellar core (e.g. Shu 1977; Shu et al. 1987; Masunaga & Inutsuka 2000), the young star grows steadily from the infalling envelope at a rate of a few 10^{-6} $M_\odot$ yr^{-1}. However, Kenyon et al. (1990) found that luminosities of most protostars fall far below those expected from energy release by steady accretion over protostellar lifetimes. This luminosity problem has since been confirmed with an improved census of protostars (e.g., Enoch et al. 2009; Dunham et al. 2010; see also discussions in Dunham et al. 2014 and Fischer et al. 2017).

The resolution of the luminosity problem likely requires a either a time-dependent or mass-dependent accretion rate (e.g., discussions in Hartmann et al. 2016 and Fischer et al. 2017; see also, e.g., Offner & McKee 2011; Myers 2012) Observationally, strong but mostly indirect evidence suggests that the accretion rate is punctuated by short bursts of rapid accretion, often termed *episodic accretion* (Kenyon et al. 1990; Dunham et al. 2010; Dunham & Vorobyov 2012). The form of this time dependence may have a lasting affect on the evolution of stars (e.g. Hartmann et al. 1997; Baraffe & Chabrier 2010; Baraffe et al. 2017; Vorobyov et al. 2017a), the physical structure of disks and their propensity to fragment, (e.g. Stamatellos et al. 2011, 2012; Vorobyov et al. 2014), and the chemistry of disks and envelopes (e.g. Kim et al. 2012; Jørgensen et al. 2013; Vorobyov et al. 2013; Visser et al. 2015; Harsono et al. 2015; Owen & Jacquet 2015; Cieza et al. 2016).

The suggestion of accretion bursts in protostars has significant support from later stages of pre-main sequence stellar evolution. Spectacular outbursts[41] with optical brightness increases of ~ 5 mag are interpreted as accre-

Astronomy, University of Central Lancashire, Preston, PR1 2HE, UK
[31] Centre for Astrophysics Research, School of Physics, Astronomy and Mathematics, University of Hertfordshire, College Lane, Hatfield AL10 9AB, UK
[32] Department of Astronomy; MC 249-17, California Institute of Technology, Pasadena, CA 91125, USA
[33] Department of Physics, Graduate School of Science, Nagoya University, 464-8602, Nagoya, Japan
[34] Korea National University of Education, Taeseongtabyeon-ro, Grangnae-myeon, Heungdeok-gu, Cheongju-si, Chungbuk 28173, Korea
[35] Department of Earth Sciences, National Taiwan Normal University, Taipei 116, Taiwan
[36] Korea University of Science and Technology, 217 Gajang-ro, Yuseong-gu, Daejeon 34113, Republic of Korea
[37] Department of Astronomy, Peking University, Yiheyuan 5, Haidian Qu, 100871 Beijing, People's Republic of China
[38] National Astronomical Observatories, Chinese Academy of Sciences, Beijing, China
[39] Department of Physics and Astronomy, Graduate School of Science and Engineering, Kagoshima University, 1-21-35 Korimoto, Kagoshima, Kagoshima 890-0065, Japan
[40] Purple Mountain Observatory, & Key Laboratory for Radio Astronomy, Chinese Academy of Sciences, 2 West Beijing Road, Nanjing 210008, China
[41] The classification scheme of EXor and FUor outbursts is some-

tion rate increases of 2-4 orders of magnitude and can last for months (called EXors following the prototype EX Lup, e.g. Herbig 2008; Aspin et al. 2010) or decades (called FUors following the prototype FU Ori, e.g. Herbig 1977; Hartmann & Kenyon 1996). Because most transient searches use optical photometry, these accretion outbursts are detected only on young stellar objects that are optically bright and are therefore biased to variability at or near the end of their main phase of stellar growth. Only a few outbursts have been detected on a deeply embedded Class 0 star (Kóspál et al. 2007; Safron et al. 2015; Hunter et al. 2017), the stage when the star should accrete much of its mass – although many FUor objects retain some envelopes and are classified as Class I objects (e.g. Zhu et al. 2008; Caratti o Garatti et al. 2011; Caratti O Garatti et al. 2016; Fischer et al. 2012; Green et al. 2013; Kóspál et al. 2017). Indirect evidence for outbursts includes chemical signatures of past epochs with high luminosity (e.g. Kim et al. 2012; Vorobyov et al. 2013; Jørgensen et al. 2015; Frimann et al. 2017) and periodic shocks/bullets along protostellar jets, which may offer a historical record of accretion events (e.g. Reipurth 1989; Raga et al. 2002; Plunkett et al. 2015). In addition to these large events, instabilities in the inner disk likely lead to more frequent but smaller bursts of accretion, as seen in more evolved disks (e.g. Costigan et al. 2014; Venuti et al. 2014; Cody et al. 2017).

Directly observing either large outbursts or accretion flickers on protostars is challenging because they are deeply embedded in dense envelopes. The accretion luminosity is not directly visible to us, and is instead absorbed by the envelope and reprocessed into photons with lower energies, which then escape from the system. Models of an accretion burst indicate that the enhanced accretion luminosity heats dust in the envelope (Johnstone et al. 2013). The dust is then seen as brighter emission at far-IR through sub-mm wavelengths. The change in luminosity is strongest at far-IR wavelengths, which traces the effective photosphere of the envelope, where the envelope becomes transparent when the local temperature drops below ~ 100 K. Single-dish observations at sub-mm wavelengths have large scales, which tends to probe the temperature structure of the outer envelope. When the protostellar luminosity increases, the outer envelope is expected to become hotter. Since the atmosphere of the Earth is opaque in the far-IR, and the most heavily embedded objects are not visible at optical/near-IR wavelengths, sub-mm observations provide us with our best ground-based window into the protostar – a snapshot of the accretion rate, averaged over the timescale of a few weeks for the luminosity burst to propagate through the envelope. While some far-IR/sub-mm variability has indeed been detected on protostars, these detections are mostly based on transients identified in optical/near-IR surveys and have few epochs of flux measurements at far-IR/sub-mm wavelengths (e.g. Billot et al. 2012; Scholz et al. 2013a; Balog et al. 2014; Safron et al. 2015; Onozato et al. 2015).

In this paper, we describe our novel James Clerk Maxwell Telescope (JCMT) survey, *A JCMT/SCUBA-2 Transient Survey of Protostars in Nearby Star Forming Regions*, shortened to *JCMT-Transient*, in which

times vague, with both classes likely including diverse phenomenon.

we use Submillimetre Common-User Bolometer Array 2 (SCUBA-2; Holland et al. 2013) to monitor the sub-mm flux of deeply embedded protostars in eight fields within nearby star forming regions. This is the first dedicated long-term sub-mm monitoring program. The only previous sub-mm monitoring programs probed variability in synchrotron radiation from the Sagittarius A* at the galactic center over five consecutive nights (Haubois et al. 2012) and the black hole X-ray binary V404 Cyg over 4.5 hrs (Tetarenko et al. 2017). Although large outbursts, with a factor of 100 increases in source luminosity, are rare (Scholz et al. 2013a; Hillenbrand & Findeisen 2015), our survey should also reveal the lower-amplitude variability (with changes of a factor or < 10 in luminosity) that are commonly detected on classical T Tauri stars. In §2 we describe our observational plans. In §3 we describe initial results, including the stability of our flux calibration. In §4, we discuss the expected contributions of this survey to our understanding of protostellar variability and related applications for this dataset. In §5 we discuss ancillary science related to disks, VeLLOs, filaments, and non-thermal emission. In §6 we discuss our expectations for the future results from this program.

2. OVERVIEW OF SURVEY METHODOLOGY

Our ongoing JCMT survey program, M16AL001, consists of monitoring 450 and 850 μm emission from eight young regions that are rich in protostars, as identified in previous Spitzer, Herschel, and SCUBA-2 Gould Belt Surveys. Sub-mm monitoring surveys have been challenging in the past because of calibration uncertainties. The wide SCUBA-2 field-of-view allows us to use multiple bright sources in the same field to calibrate the image relative to other bright objects in the field, the sub-mm equivalent of differential photometry.

2.1. *Sample Selection*

We selected eight 30′ regions of nearby (< 500 pc), active star formation to maximize the number of protostars and disks in the fields, with a preference to the youngest regions while also avoiding regions with the most complex, confused features. The fields include a total of 182 Class 0/I objects, 132 flat-spectrum objects, and 670 disks (see Table 1), as previously classified from Spitzer SEDs by Dunham et al. (2010), Stutz et al. (2013), and Megeath et al. (2016). Each region includes 3–41 peaks with 850 μm fluxes above 0.5 Jy/beam and 12–120 peaks above 0.12 Jy/beam, and 3–14 protostars associated with those peaks. All requested fields have a past epoch from the JCMT Gould Belt Survey (Ward-Thompson et al. 2007), along with complementary Spitzer mid-IR (Dunham et al. 2015; Megeath et al. 2016) and Herschel far-IR imaging (André et al. 2014).

2.2. *Observing Strategy*

The SCUBA-2 instrument is a 10,000 pixel bolometer camera that images simultaneously at 450 and 850 μm with 9″8 and 14″6 resolution (Holland et al. 2013; Dempsey et al. 2013). Both focal planes consist of four subarrays of 1280 bolometers that simultaneously cover a field with an $\sim 8'$ diameter. The regions are observed in a pong 1800″ pattern, in which SCUBA-2 scans over a field-of-view of 30′ diameter to produce an image with smooth sensitivity across the map (Kackley et al. 2010).

Our observations are being obtained in weather bands 1–3, which correspond to different levels of atmospheric H_2O column densities that lead to opacities of $\tau < 0.12$ at 225 GHz. Mairs et al. (2017) provides a complete list of observations obtained through February 2017, including τ and sensitivity. To date, 21% of our observations have been obtained in Band 1 (the driest weather, $\tau < 0.05$ at 225 GHz) and 39% have been observed in Band 2 ($0.05 < \tau < 0.08$). The exposure time for each individual epoch is 20–40 min., adjusted for the atmospheric opacity to achieve a sensitivity of 12 mJy/beam per 3″ square pixel at 850 μm.[42] Each field is being observed once per month when available, with the first observations obtained in December 2015 and an initial program that runs through January 2019. Since JCMT operations can extend a few hours into dawn, each field will be observed ~ 10 times per year. When all images are stacked, the total sensitivity at 850 μm will be ~ 2.5 mJy/beam (compared to ~ 4 mJy/beam for the Gould Belt Survey, Mairs et al. 2015).

This monthly cadence is selected based on estimates of how quickly a luminosity burst would propagate through the envelope and be detectable, following the radiative transfer and envelope models calculated by Johnstone et al. (2013). Because sub-mm photons from an envelope are emitted from a large volume, the light propagation time is a few weeks. Once irradiated, the dust heating timescale is negligible because dust has a low heat capacity. Therefore, a 1-month cadence is selected as the estimated optimal cadence for sensitivity to accretion variability on weeks-months timescales. This cadence will also allow us to stack several images over a few months to characterize any smooth long term changes in the flux and to evaluate variability of fainter objects in our field. This stacking will reduce the flux calibration uncertainties introduced stochastically by changes of the optical depth of the atmosphere on timescales shorter than the integration time.

2.3. *Data Reduction and Source Extraction*

A full description of the data reduction and flux calibration is provided in the companion paper by Mairs et al. (2017), following on the methods developed by Mairs et al. (2015) and filtering on scales of 200″. Compact peaks are measured using the JCMT Science Archive algorithm JSA_catalogue (see the PICARD package in Starlink, Gibb et al. 2013, and Appendix A). These peaks are not fully vetted. Appendix A includes only those peaks that are established to be associated with a nearby disk or protostar, with a sub-mm centroid located $< 7''$ from the centroid of the mid-IR peak (see Appendix A for further details).

Since flux variability will be converted into a change in protostellar accretion luminosity, the accuracy of our flux calibration determines our sensitivity to accretion events. Standard flux calibration for sub-mm imaging with SCUBA-2 (and other similar instruments) is calculated from contemporaneous observations of flux standards and simultaneous measurements of the atmo-

---

[42] This paper quotes sensitivities as pixel-to-pixel variation derived using a beam size of 14.6 arcseconds and a pixel size of 3 arcseconds, which is consistent with the sensitivities in Mairs et al. (2017) but may differ from methodologies in other studies.

TABLE 1
DESCRIPTION OF THE EIGHT SELECTED FIELDS

Name	Location	dist	# of Peaks[a]				Spitzer Sources[b]			Class 0/I[c]		Disks[c]	
		pc	> 0.125	> 0.25	> 0.5	> 1.0	0/I	Flat	II	> 0.125	> 0.5	> 0.125	> 0.5
Perseus - NGC 1333	032854+311652	270[d]	33	24	10	6	34	14	62	14	6	1	0
Perseus - IC348	034418+320459	303[d]	12	4	3	2	13	8	114	5	3	0	0
Orion A - OMC2/3	053531-050038	388[e]	120	77	41	25	64	–	600	12	10	12	4
Orion B - NGC2024	054141-015351	423[e]	38	14	8	4	26	–	232	3	2	1	0
Orion B - NGC2068	054613-000605	388[e]	31	24	12	5	22	–	117	9	6	0	0
Ophiuchus	162705-243237	137[f]	41	23	7	3	21	30	87	12	1	6	2
Serpens Main	182949+011520	436[g]	16	15	10	7	19	9	51	8	7	0	0
Serpens South	183002-020248	436[g]	51	27	14	2	50	34	142	10	1	1	0

[a]# of individual peaks with SCUBA-2 850 μm flux brighter than listed.
[b]Total # of protostars in field, as identified by Stutz et al. (2013), Dunham et al. (2015), and Megeath et al. (2016).
[c]Protostars and disks located within $7''$ of a peak, see also Appendix A
[d]This work using parallaxes from the Gaia DR1 TGAS catalogue.
[e]Parallaxes from the VLBI GOBELINS program (Kounkel et al. 2017).
[f]Parallax from the VLBI GOBELINS program (Ortiz-León et al. 2017a).
[g]Parallaxes from the VLBI GOBELINS program (Ortiz-León et al. 2017b).

spheric opacity. This standard approach to flux calibration is accurate to $\sim 7 - 10\%$ (Dempsey et al. 2013).

To improve upon this standard approach, we leverage the presence of many protostars within single sub-mm fields to improve the accuracy of our fluxes by calibrating the fluxes relative to other sources in the same image. A set of stable, bright peaks is identified within each field and then used to provide the relative calibration for each image, achieving a flux accuracy of $\sim 2 - 3\%$ (Mairs et al. 2017). This quantified uncertainty also establishes the confidence level that any detected variability is attributed to the source, rather than possible contributions because of changes in atmospheric transmission. For faint targets, images will be stacked to look for variability on longer timescales.

Our science results to date focus on 850 μm images. Imaging at 450 μm is sensitive to objects in our field only during observations obtained with low precipitable water vapor (Band 1 or Band 2 weather, about 60% of epochs). Since our techniques for quantifying variability require many epochs per field, analyses of 450 μm images will occur after we have obtained enough imaging in the best weather bands and developed techniques for the analysis of 850 μm images.

3. DESCRIPTION OF FIELDS AND SOURCES

The eight star-forming regions in this survey were chosen as follows. We analyzed the JCMT Legacy Release Peak Catalogue of observed 850 micron sub-mm peaks (Graves et al. submitted) to find $30''$-wide fields with the largest number of sub-mm sources, using these as a proxy for star formation activity. Typically the brightest (most massive) sub-mm peaks in star-forming regions are found to be associated with deeply embedded protostars (e.g. Jørgensen et al. 2007, 2008) and are interpreted as the molecular core out of which the star is forming. A subset of these bright (massive) peaks are not known to harbor protostars and are interpreted as being at an earlier evolutionary stage, i.e. starless or prestellar (see, e.g., Sadavoy et al. 2010 and Pattle et al. 2015, 2017). As the sub-mm peaks get fainter (lower envelope mass), the association with protostars diminishes, although the mass function of the starless cores subset suggests that they may still be related to the star formation process

(e.g. Motte et al. 1998). Many of the fainter peaks may be wispy structure within the molecular cloud and not directly related to ongoing star formation. Some fainter emission peaks may be disks associated with Class II protostars.

Figure 2 and Table 1 show the total number of sources with peak 850 μm flux brighter than 0.125 Jy/beam for all regions in our survey, sorted by brightness bin and by association with protostars and disks (see also Appendix A). To better understand the distribution of protostellar cores versus starless cores in our regions, we collated the sub-mm peaks against catalogues of known protostars (Class 0/I objects) and disks (Class II objects), as identified in past Spitzer photometry (Dunham et al. 2015; Megeath et al. 2016) as well as extensive sub-mm imaging (e.g. Johnstone & Bally 1999; Hatchell et al. 2005; Kirk et al. 2006; Johnstone et al. 2006; Enoch et al. 2006, 2007). Of the 342 bright peaks, 73 are associated with known protostars (Class 0/I) and 20 are associated with known disks (Class II). Given the poor resolution of the JCMT, some of these associations may be coincidental, particularly in the case of disks (most of which are too faint to be detected with our sensitivity). Moreover, since the determination of protostellar class is often ambiguous, some sources identified as disks are more deeply embedded sources, if for example the source is viewed through a hole in the envelope. Similarly, some of the most deeply embedded protostars are missed by the surveys due to extreme extinction, even in the mid-IR, so the lack of association of a peak with a known protostar does not rule out the presence of a protostar within the peak. Indeed, Stutz et al. (2013) found a few PACS Bright Red Sources (PBRs) objects at 70 μm with Herschel that were entirely unseen with Spitzer. Given these caveats, the numbers presented here should provide a reasonable measure of the degree of star formation activity taking place in the observed peaks in our survey, but any variability that we uncover will require more careful consideration of the individual peak and any neighboring protostar.

The following subsections describe each region in more detail.
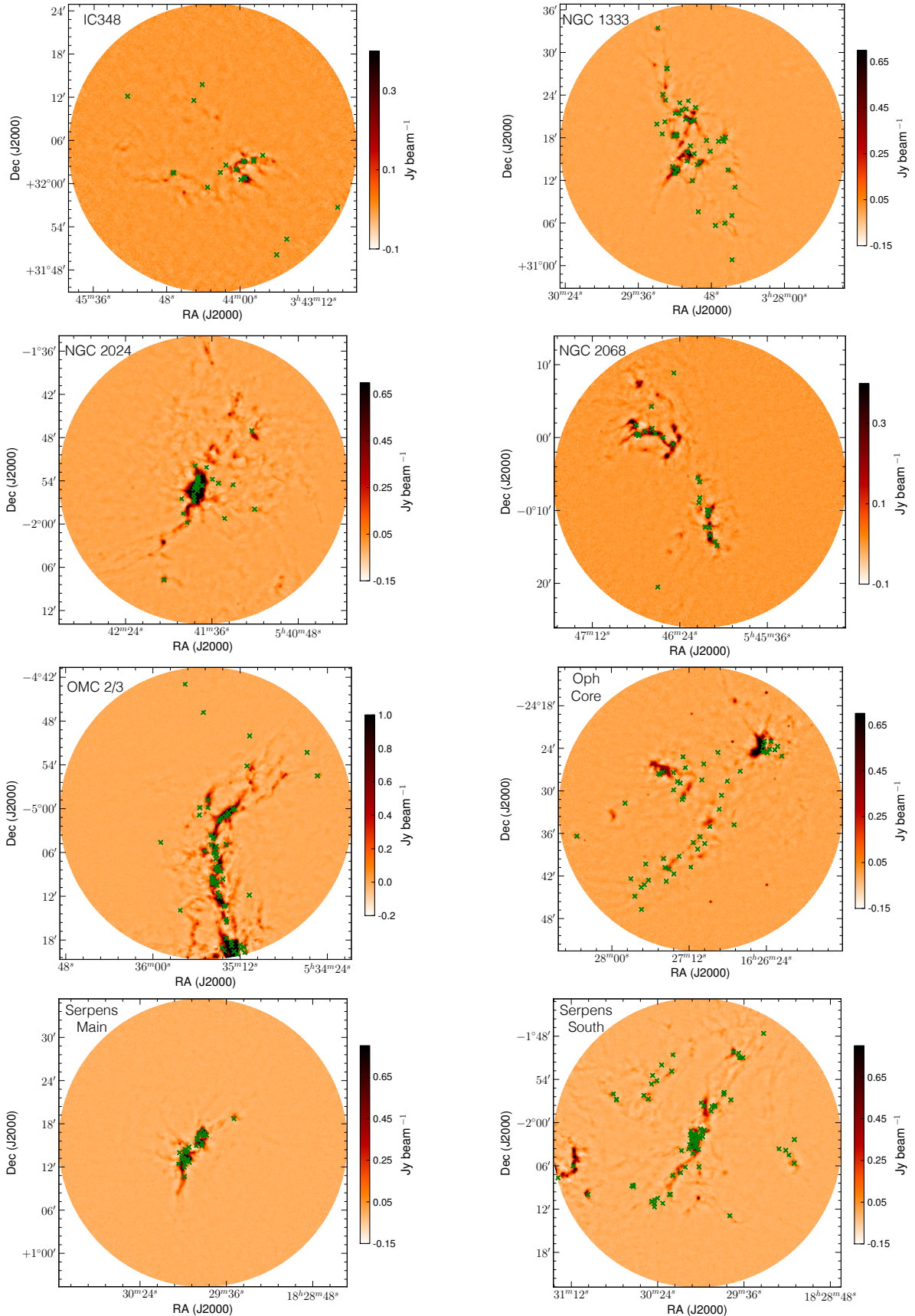
3.1. NGC 1333 – Perseus

FIG. 1.— The SCUBA-2 850 μm images of all eight regions in our survey, co-added over the first year of data (see also Mairs et al. 2017). The marks show the location of Class 0, Class I, and flat spectrum protostars, as identified and classified by Dunham et al. (2015) and Megeath et al. (2016).

NGC 1333 is in many ways a prototypical nearby star forming cluster, with a mass of 450 $M_\odot$ and with a diameter of $\sim 1-2$ pc, located within the large-scale Perseus star forming complex (e.g. Bally et al. 2008; Walawender et al. 2008). The temperatures of the regions in NGC 1333 range from 10–14 K for filaments and ambient cloud material, are ~ 20 K on the southern edge of the cloud, and reach 40 K near the B star SVS3 and the embedded protostar IRS 6 (Hatchell et al. 2013; Chen et al. 2016). The distance estimated from the Gaia TGAS catalogue (Gaia Collaboration et al. 2016)[43] of 271 ± 20 pc is consistent with previous distance estimates of 220–320 pc (see discussion in Scholz et al. 2013b) and would imply that NGC 1333 is located in the foreground of the Perseus star forming cloud.

Members range from 2 massive B-stars down to objects with estimated masses of a few Jupiter masses, with a distribution consistent with a single power law from low-mass stars to brown dwarfs (Scholz et al. 2012b,a; Rebull et al. 2014; Luhman et al. 2016). Gutermuth et al. (2008a) found that $\sim 30\%$ of stars with a mid-IR excess are embedded Class I protostars, which when combined with a lack of a strong central condensation and localized extinction together point to an early evolutionary state for the cloud. The commonly-adopted age of 1–2 Myr for NGC 1333 is slightly younger than that of IC 348, although isochrone fits to optical/near-IR members do not show a significant age difference between the two clusters (Luhman et al. 2016). NGC 1333 also harbors several dozen Herbig-Haro objects (e.g. Bally et al. 1996; Yan et al. 1998) with associated molecular line emission (Knee & Sandell 2000; Curtis et al. 2010).

3.2. IC 348 – Perseus

IC 348 is a nearby star cluster associated with the Perseus cloud complex and is located at ~ 303 pc from parallax measurements.[44] With an average age of 3–5 Myr (e.g. Luhman et al. 2016), IC 348 is older than the other regions in this survey and was selected because of the high density of protostellar disks within the field-of-view, along with a few protostars. Thirteen disks were detected in previous deep SCUBA-2 images of 850 μm emission (Cieza et al. 2015). Southwest of the main cluster is a protostellar cluster, with dense molecular clouds, Class 0/I protostars and Herbig-Haro objects (e.g. Walawender et al. 2006).

3.3. OMC-2/3 – Orion

The Orion Molecular Cloud 2/3 region (OMC-2/3) is located in the northern part of the Orion Molecular Cloud (OMC, Bally et al. 1987; Mezger et al. 1990) and is often referred to as the integral-shaped filament (Johnstone & Bally 1999; Salji et al. 2015; Lane et al. 2016). Our pointing includes the northern half of the integral-

shaped filament and contributes roughly 40% of the total number of bright peaks in our survey. The OMC 2/3 region, located at ($d = 388$ pc from the GOBELINS VLBI parallax survey; Kounkel et al. 2017), is one of the best-studied and richest nearby star-forming regions at all observable wavelengths (e.g. Johnstone & Bally 1999; Tsujimoto et al. 2002; Megeath et al. 2012) and has a disk/envelope fraction of 20% (e.g. Chini et al. 1997; Nutter & Ward-Thompson 2007; Peterson et al. 2008; Megeath et al. 2012; Takahashi et al. 2013). Two sources in this region are deeply embedded PACS Bright Red Sources (PBRs) identified using far-IR photometry (Stutz et al. 2013; Tobin et al. 2015). This region also includes (arguably) the first detected outburst of a Class 0 protostar (Safron et al. 2015). Most protostars are located along the densest part of the molecular filaments, while Class II sources are distributed over the region. Sub-mm CO emission line surveys have revealed ~ 15 molecular outflows within this region (Aso et al. 2000; Williams et al. 2003; Takahashi et al. 2008, 2012).

3.4. NGC 2024 – Orion

NGC 2024 (the Flame Nebula) is located within the Orion B (L1630) cloud complex, one of the nearest active high-mass star-forming regions (see review by Meyer et al. 2008), located at a distance of ~ 388 pc (Kounkel et al. 2017). The region is one of the densest of all clouds in Orion, with a protostellar density of ~ 50 pc^{-2} (Skinner et al. 2003; Megeath et al. 2016) spread over a virial radius of 0.4 pc (Lada et al. 1997). A long molecular ridge corresponds to the regions of highest extinction and includes many dense cores (e.g. Thronson et al. 1984; Visser et al. 1998; Choi et al. 2012). Within the molecular ridge, two clumps of protostars are especially bright in sub-mm dust continuum emission, revealing a total mass of 633 $M_\odot$ (Johnstone et al. 2006; Kirk et al. 2016).

3.5. NGC 2068 and HH 24 – Orion

NGC 2068 and HH24 (together referred to as NGC 2068 throughout this paper) are also located within the Orion B cloud complex, with HH 24 to the south of NGC 2068 (Kutner et al. 1977; Bontemps et al. 1995; Gibb 2008). The census of near-IR and mid-IR protostars leads to total masses of NGC 2068 and HH 24 of $\sim$ 240 $M_\odot$ and 120 $M_\odot$, respectively (Spezzi et al. 2015). The protostellar population includes several PBRs (e.g. Stutz et al. 2013) and the eruptive protostar V1647 Ori (also known as McNeil's nebula; Reipurth & Aspin 2004).

3.6. Ophiuchus Core

The Ophiuchus molecular cloud spans 30 pc^2 on the plane of the sky and contains over 3000 solar masses of gas (e.g. Wilking et al. 2008; Dunham et al. 2015). Star formation in the Ophiuchus complex may have been triggered by the Sco-Cen OB association, and includes numerous streamers of molecular gas pointing away from Sco-Cen (e.g., Vrba 1977; Loren & Wootten 1986; Wilking et al. 2008). The parallax distance adopted here of 137 pc from the GOBELINS survey (Ortiz-León et al. 2017b) is slightly larger than previous distance measurements of ~ 120 pc to the cluster (Loinard et al. 2008).

The most active portion of the Ophiuchus cloud complex is L1688, which stands out from other nearby low

---

[43] The Gaia TGAS DR1 catalogue contains 2 likely members within 15' of the cluster centre with distances of 274^{+18}_{-20} pc and 267^{+19}_{-21} pc (Gaia Collaboration et al. 2016).

[44] Five members of IC348 are in the Gaia DR1 TGAS catalog (Gaia Collaboration et al. 2016), with an average parallax distance of 303 ± 21 pc, where the uncertainty is dominated by the systematic error of ~ 0.3 mas. This distance is consistent with past measurements from Hipparcos (van Leeuwen 2007) and other methods (see discussion in Herbst 2008).

mass star forming regions because the star forming environment is more clustered (Motte et al. 1998; Johnstone et al. 2000; Allen et al. 2002; Johnstone et al. 2004; Young et al. 2006; Stanke et al. 2006). L1688 shows significant substructure, with 13 identified peaks, many of which contain multiple starless and protostellar cores (Loren et al. 1990; Motte et al. 1998; Kamazaki et al. 2001; Johnstone et al. 2004; Young et al. 2006; Stanke et al. 2006; Nakamura et al. 2012; White et al. 2015; Pan et al. 2017). The Oph A clump, in the northwest corner of L1688, has the highest column densities and temperatures (Motte et al. 1998; Johnstone et al. 2000; Friesen et al. 2009; Pon et al. 2009; Pan et al. 2017), and appears as a bright crescent of continuum emission wrapping around the position of the nearby B star S1 (Elias 1978). The prototype for the class 0 protostellar stage, VLA 1623 (André et al. 1993), is located within this field.

3.7. *Serpens Main*

The Serpens Main region is an active star forming region (Strom et al. 1976; Eiroa et al. 2008) with a total mass of 230–300 $M_\odot$ (Olmi & Testi 2002; Graves et al. 2010) located at 436 ± 9 pc (from the GOBELINS survey Ortiz-León et al. 2017b). The SE and NW substructures are bright in sub-mm/mm dust continuum emission (Casali et al. 1993; Davis et al. 1999; Kaas et al. 2004). The protostars and ongoing star formation in Serpens Main is highly concentrated at the center of our pointing. The sources in early evolutionary stages (Class 0/I and Flat SEDs) are clustered in small regions while the older Class II and III sources are distributed outside of these clusters (Harvey et al. 2007).

The velocity field of Serpens Main shows the presence of global infall motion, outflow, rotation, and turbulence (Olmi & Testi 2002). The velocity field in the NW subcluster is relatively uniform, on the other hand, while the SE subcluster has a more complicated velocity structure showing a large velocity dispersion (>0.5 km s^{-1}) at the central region (Graves et al. 2010; Duarte-Cabral et al. 2010; Lee et al. 2014). The NW subcluster includes known IR-variables OO Ser, EC 53, and EC 37 (Hodapp 1999; Kóspál et al. 2007; Hodapp et al. 2012). Sub-mm variability of the protostar EC 53, which was uncovered in this survey, will be presented in Yoo et al. (2017).

3.8. *Serpens South*

Serpens South is an active star-forming region within the Aquila Rift molecular complex, located at 436 ± 9 pc (Ortiz-León et al. 2017b) and ~3° south of Serpens Main (Kern et al. 2016). Gas is flowing inward onto the filaments to supply the fuel for star-formation (Kirk et al. 2013). Maury et al. (2011) measure a total mass of the cluster of ~ 1660 $M_\odot$, adjusted for the updated distance (see Friesen et al. 2016). The ratio of Class 0/Class I sources of ~ 77% and the Class I to Class II ratio of about 80% are among the highest fractions for nearby star forming regions (Gutermuth et al. 2008b; Maury et al. 2011).

4. TESTING MODELS OF PROTOSTELLAR ACCRETION

During protostellar accretion, viscous processes in the disk transport angular momentum outwards, allowing gas to flow inwards towards the protostar. The source of
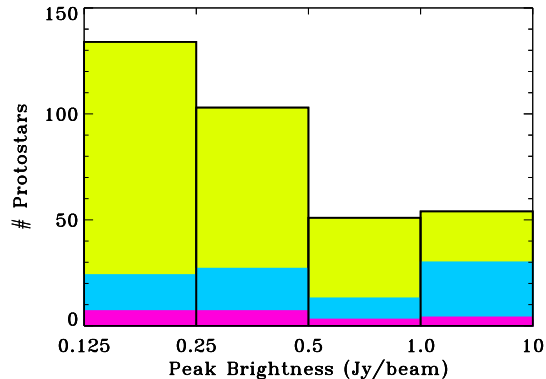

FIG. 2.— The distribution of 342 peaks with 850 μm peak brightness above 0.125 Jy/beam for all eight regions in our survey (yellow). The purple and blue histograms respectively show the number of peaks associated with one or more disks and protostars. Based on the analysis of Mairs et al. (2017), we can achieve 2–3% accuracy for the 105 peaks brighter than 0.5 Jy/beam and 10% for the 237 sources with brightness 0.125–0.5 Jy/beam. Of these 342 peaks, 93 are associated with distinct protostars or disks. In some cases, multiple protostars are blended together to form a single peak at the resolution of JCMT.

viscosity in protostellar disks is uncertain (e.g. Armitage 2015; Hartmann et al. 2016); it could be due to turbulence or instabilities (gravitational, magneto-rotational) that develop where the conditions are right. When the accretion rate through some radius in the disk is lower than the accretion rate at larger radii, material builds up until the accretion rate through the inner disk adjusts. A steady accretion flow through the disk and onto the star is determined by the most stringent bottleneck, with short periods of strong accretion when that bottleneck breaks. Both the amplitude of the non-steady accretion and the timescale over which the accretion varies are likely to span a wide range of values. Models of these accretion processes provide predictions for the frequency and amplitude of accretion variability, with limitations related to physical scales and MHD microphysics.

Prospects for detecting accretion variability depend on the size and location of instabilities within the disk. In the past, outbursts on young stars have been differentiated into EXors and FUors based on timescales and spectral characteristics, although it remains unclear whether these events have different physical causes or are simply different manifestations of similar phenomena (e.g. Audard et al. 2014). Several mechanisms have been proposed to explain short- and long-term variability, including gravitational instabilities in the outer disc region (Vorobyov & Basu 2005, 2015; Machida et al. 2011), thermal instabilities in the inner disc region (Hartmann & Kenyon 1985; Lin et al. 1985; Bell et al. 1995), a combination of gravitational instabilities in the outer disc region and the magneto-rotational instability in the inner disc region (Armitage et al. 2001; Zhu et al. 2009, 2010), spiral-wave instabilities (Bae et al. 2016; Hennebelle et al. 2017), gravitational interactions with companions or passing stars (Bonnell & Bastien 1992; Forgan & Rice 2010; Green et al. 2016; Muñoz & Lai 2016),
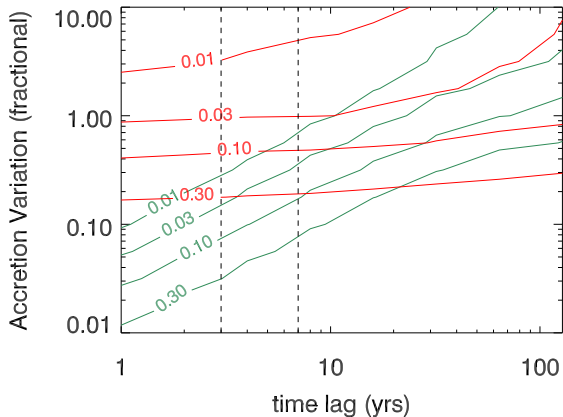
FIG. 3.— The expected fraction of time that a given theoretical model returns an amplitude variation greater than a specific amount as a function of the time lag between observations. The green contours show results for a Vorobyov & Basu (2010) model in which accretion variability is driven by large-scale modes within the gravitationally-unstable disk. The red contours show result for a Bae et al. (2014) model in which accretion variability is driven by the activation of the magneto-rotational instability in the otherwise magnetically inert inner disk, via heating from gravitational instability-driven spiral waves. The contours are labeled with the fraction of stars that would show the level of variability. In both models, larger amplitudes correlate with longer times. The dashed lines denotes a three-year separation in time for our survey and a seven-year separation in time between earlier epochs from the JCMT Gould Belt Survey and the end of our survey.

and magnetospheric instabilities (e.g. D'Angelo & Spruit 2010; Romanova et al. 2013; Armitage 2016). Some of these processes lead to the rare accretion bursts of FUors and the much more common variation of accretion seen on classical T Tauri stars (e.g. Venuti et al. 2014; Costigan et al. 2014; Cody et al. 2017), while others may cause periodic accretion bursts, as seen in a few objects (Hodapp et al. 2012; Muzerolle et al. 2013; Hodapp & Chini 2015).

While only some of these theoretical ideas are capable of providing significant mass accretion variability over the lifetime of embedded protostars, all should produce observable signatures in accretion luminosity with characteristic amplitudes and timescales. Assuming that accretion is related to disk transport processes on orbital timescales, the variability will depend on the radii where the physical transport processes originate and will range from days in the inner disk to hundreds of years in the outer disk. Within deeply embedded protostars, the range of accretion events taking place is almost entirely unconstrained from both theoretical and observational perspectives.

Monitoring the brightness of deeply embedded protostars with a flux calibration uncertainty of 2–3% (Mairs et al. 2017) will produce direct measurements of both the range of accretion events and their duration, provided that the duration is longer than a few days and that the accretion is radiative and not optically-thick. Since the total luminosity change is ~ 10 times larger than any change expected from the dust continuum emission at 850 μm (Johnstone et al. 2013), a 3% calibration uncertainty corresponds to a $\sim 30\%$ uncertainty in the protostar luminosity. The power spectrum of accretion

variability on young objects will then provide a diagnostic for the size and location of disk instabilities (Elbakyan et al. 2016), independent of whether the majority of the mass is accreted in rare large events. In addition to these changes from accretion luminosity, single-epoch brightness increases may be detected from any star in our field and attributed to either short accretion bursts or non-thermal synchrotron emission (see §5.4).

Our monitoring of 342 peaks brighter than 0.125 mJy/beam (73 of which are associated with protostars and 20 with disks) will then provide an unbiased survey of variability on a large enough dataset for robust statistical analyses. The starless cores should not be variable and therefore provide a control sample in statistical analyses. Within our fields, 176 more protostars are fainter than 0.125 mJy/beam but increase the sample size for a search for flux increases of factors of 2–10. While these large bursts are expected to be rare, models of accretion variability suggest that annual variations of 10% may be common. Figure 3 presents this analysis as applied to the outburst models of Bae et al. (2014) and Vorobyov & Basu (2015), with clear differences in the observational signatures of accretion variability on short (less than five year) timescales that result from the different input physics. In the Bae model, $> 30\%$ of sources will vary by 10% (our 3-σ detection limit) over our 3.5 year program, while in the Vorobyov & Basu model $\sim 7\%$ of sources would be variable at the 10% level. Vorobyov & Basu (2015) predict that fewer bursts should occur during the Class 0 stage than during the Class I stage.

These values suffer from large uncertainties because neither model was designed to resolve short timescales or the small distances over which the last steps of accretion occur. However, they provide some guidance on how this program could be used as a test of models for disk accretion. Moreover, a non-detection of variability on this sample would indicate that the accretion flow moves smoothly through the inner disk, placing a stringent requirement on the instability physics in the inner disk at young ages.

Our initial investigations will search for short-term variability, as found in EC 53 (Yoo et al., in prep), and will also place limits on the stability of bright objects in our sample over the first year of our program and in comparison to the Gould Belt Survey observations obtained $\sim 3 - 4$ years ago (Mairs et al., in prep). Once our survey is completed, we will analyze all 450 and 850 μm imaging from our survey plus the Gould Belt Survey to identify any long-term secular changes during our ~ 3 years of monitoring, and with ~ 7 year time baselines when including the Gould Belt Survey.

5. RELATED SCIENCE GOALS

After our first year of data, the stacked image from each region yields a 1σ noise level of ~ 4 mJy/beam at 850 μm, similar to the depth of SCUBA-2 imaging from the JCMT Gould Belt Survey (Mairs et al. 2015) and to the deep SCUBA-2 disk surveys in the σ Ori, λ Ori, and IC 348 star-forming regions (Williams et al. 2013; Ansdell et al. 2015; Cieza et al. 2015). The final stacked image after three years of monitoring should achieve a sensitivity of ~ 2.5 mJy/beam. These deep images will be useful for studying very low luminosity protostars, faint filamentary structures, disks, and non-thermal syn-

chrotron emission, as described below.

5.1. *Very Low Luminosity Objects (VeLLOs)*

Very Low Luminosity Objects (VeLLOs) are protostars with luminosities ≤ 0.1 L$_\odot$, first discovered in *Spitzer* observations of cores thought at the time to be starless (e.g. Young et al. 2004; Bourke et al. 2006; Dunham et al. 2008; Hsieh et al. 2015). Their very low luminosities are explained by either low accretion rates or low protostellar masses, if they are proto-brown dwarfs (e.g. Lee et al. 2009, 2013; Hsieh et al. 2016). The class of VeL-LOs may even include some first cores, which have short lifetimes of 10^3 yr before the protostar is created (Larson 1969; Masunaga & Inutsuka 2000). Using coupled disk hydrodynamics and stellar evolution models, Vorobyov et al. (2017b) demonstrate that the characterization of VeLLOs depends on the energy of the gas accreted onto the central object. VeLLOs are only expected to occur if some time intervals have very low accretion rates, thereby implying other times have high accretion rates. Our observations will reach a 3σ sensitivity of $\sim 10^{-3}$ M$_\odot$ in envelope mass (depending on temperature and opacity) for all regions, and should therefore be capable of unambiguously identifying proto-brown dwarfs in our target fields. The factor of 2 improvement in sensitivity in our survey relative to the Gould Belt Survey should reveal many more of these faint objects than are detected in the Gould Belt Survey.

5.2. *Protoplanetary Disks*

For young stars that have dispersed their envelope, a sensitivity of ~ 2.5 mJy/beam will lead to detections of disks with ~ 1 Earth mass of dust in Ophiuchus and 10 Earth masses in the more distant Orion region, assuming standard conversions between sub-mm emission and dust mass (e.g. Andrews et al. 2013). Large area SCUBA-2 maps of similar depth in the older σ Ori and λ Ori regions have revealed that most infrared-Class II disks have very low masses at 3–5 Myr (Williams et al. 2013; Ansdell et al. 2015), and constrain planet formation timescales more strongly than infrared surveys; similar results have been obtained from recent ALMA surveys (Ansdell et al. 2016; Barenfeld et al. 2016; Pascucci et al. 2016) and from younger regions in the Gould Belt Survey (e.g. Dodds et al. 2015; Buckle et al. 2015). Our unbiased search for disks in some of the youngest regions of nearby star-formation will complement the past results from older regions to establish the evolution of the disk dust mass distribution versus evolutionary stage.

5.3. *Filamentary Structure*

Much of the mass in star-forming regions is located in filamentary structures (e.g. André et al. 2014). While a full understanding requires a combination of column density and velocity information, much can be learned from dust continuum observations alone. Herschel analyses (e.g. Arzoumanian et al. 2011) have suggested that filaments have a characteristic width of 0.1 pc. However, the filament width may be influenced by telescope resolution, since JCMT Gould Belt images of the Orion A molecular cloud revealed that many filaments are significantly narrower than 0.1 pc (Salji et al. 2015; Panopoulou et al. 2017). Many filaments appear to have significant substructure along both their long and short axes and may be bundles of sub-filaments or fibers, which have been rarely analyzed in detail but may hold important clues to the stability and nature of the filaments (Contreras et al. 2013; Hacar et al. 2013, 2017). Deeper SCUBA-2 observations with JCMT resolution will better reveal faint extended substructure, thereby extending the range of filaments to those that are lower mass and less dense, and will allow for a robust measurement of filament widths. Extended structures on scales of $> 600''$ are filtered out during data reduction to account for atmospheric changes during the observations.

The filamentary structure obtained with our deep co-added integrations will also be compared with the orientation of outflows within these regions to examine the orientation of disks in filamentary environment. Recent results have shown axisymmetric flattened envelopes around Class 0 sources (Lee et al. 2012), while outflows are often seen perpendicular to the direction of the filament (e.g. Tobin et al. 2011). Statistics for outflows emanating from protostars that are still within their birth filamentary structures will test whether these expectations are correct, as a way to constrain the angular momentum evolution of protostars.

5.4. *Non-thermal Emission from Young Stars*

Young stars are magnetically active, producing X-rays and synchrotron emission with a steady and a time-variable component (Güdel 2002; Forbrich et al. 2017). Flares at mm and cm wavelengths are thought to be produced by either accretion variability or by high-energy events, which produce synchrotron emission from relativistic electrons gyrating in magnetic fields (Bower et al. 2003; Massi et al. 2006). The time-variable component appears as flares that have been seen in several sources to wavelength as short as 3 mm (e.g. Bower et al. 2003, 2016; Salter et al. 2010; Kóspál et al. 2011), and may extend into the sub-mm due due to synchrotron self-absorption (Bower et al. 2003; Massi et al. 2006). In a few cases, correlated X-ray and infrared variability may suggest that variability of high-energy emission and accretion outbursts are not necessarily distinct phenomena (e.g. Kastner et al. 2006).

This SCUBA2 monitoring program will provide important links to longer wavelengths in the emerging context of YSO variability at infrared, X-ray, and centimeter radio wavelengths (e.g Forbrich et al. 2015, 2017). Sub-mm emission flares detected from diskless stars would be directly attributable to magnetic activity, thereby providing constraints on the electron energy distribution and the energetics of the excitation mechanism for these events. Such flares may also contaminate single-epoch sub-mm flares from protostars, though the spectral index of the 450 to 850 μm emission (if observed in good weather conditions) may allow us to discriminate between a non-thermal emission flare and a brief protostellar outburst.

6. SUMMARY AND FUTURE PERSPECTIVES

Our ongoing sub-mm transient search is a novel science experiment. We are using JCMT/SCUBA-2 to monitor once per month the 450 and 850 μm emission from eight $30'$ fields within nearby star-forming regions. The full survey area of 1.6 sq. deg. includes 105 peaks at 850

μm brighter than 0.5 Jy/beam and 237 additional peaks brighter than 0.125–0.5 Jy/beam. Of these peaks, 93 are associated with distinct protostars or disks. In addition, 176 more protostars are fainter than 0.125 Jy/beam but increase our chances of detecting large sub-mm eruptions. The flux calibration leverages the high density of sources in each field and is now reliable to $2 - 3\%$ for bright sources, as expected for the 12 mJy/beam sensitivity of our images (Mairs et al. 2017). This sub-mm version of differential photometry allows us to confidently quantify the stability of sub-mm sources and identify any outliers. Our survey is the first systematic, far-IR/sub-mm transient monitoring program dedicated to evaluating the variability on protostars on timescales longer than a year.

Protostellar outbursts are most often found in wide-field optical transient searches, such as the Palomar Transient Factory and ASAS-SN (e.g. Miller et al. 2011; Holoien et al. 2014). Some variability studies, such as the VVV survey and YSOVar, have targeted specific regions in the near- and mid-IR (e.g. Contreras Peña et al. 2017; Cody et al. 2014). However, these optical/near-IR searches are not sensitive to the most embedded (youngest) objects and include brightness changes related to variability in the line-of-sight extinction (e.g. Aspin 2011; Hillenbrand et al. 2013), while sub-mm luminosity should change only as the result of a variation in the protostellar luminosity.

When we began this program, we were uncertain whether any embedded young sources would show sub-mm variability. While outbursts detected at optical/near-IR wavelengths are rare (Scholz et al. 2013a; Hillenbrand & Findeisen 2015), outbursts may be much more common at younger evolutionary phases since the disks are constantly accreting from their envelopes and may need to redistribute mass to maintain stability. However, some models of protostellar evolution predict a lack of strong outbursts in the Class 0 phase (e.g. Vorobyov & Basu 2015).

Within our first year, periodic sub-mm emission has already been measured from a Class I source and will be published in a companion paper (Yoo et al. in prep.); other sources show potential long-term trends. Our future efforts will establish the frequency and size of outbursts during our 3.5 yr survey, and also by comparing our first year of data to the previous epoch of SCUBA-2 450 and 850 μm imaging from the JCMT Gould Belt Survey to extend time baselines to ~ 7 yr (Mairs et al. in prep). By the end of our program, the range of variability in our sample will be able to probe the scale of disk instabilities relevant on months- and years-long timescales.

REFERENCES

Allen, L. E., Myers, P. C., Di Francesco, J., et al. 2002, ApJ, 566, 993

André, P., Di Francesco, J., Ward-Thompson, D., et al. 2014, Protostars and Planets VI, 27

André, P., Ward-Thompson, D., & Barsony, M. 1993, ApJ, 406, 122

Andrews, S. M., Rosenfeld, K. A., Kraus, A. L., & Wilner, D. J. 2013, ApJ, 771, 129

Ansdell, M., Williams, J. P., & Cieza, L. A. 2015, ApJ, 806, 221

Ansdell, M., Williams, J. P., van der Marel, N., et al. 2016, ArXiv e-prints, arXiv:1604.05719

Armitage, P. J. 2015, ArXiv e-prints, arXiv:1509.06382

—. 2016, ApJ, 833, L15

Armitage, P. J., Livio, M., & Pringle, J. E. 2001, MNRAS, 324, 705

Arzoumanian, D., André, P., Didelon, P., et al. 2011, A&A, 529, L6

Aso, Y., Tatematsu, K., Sekimoto, Y., et al. 2000, ApJS, 131, 465

Aspin, C. 2011, AJ, 142, 135

Aspin, C., Reipurth, B., Herczeg, G. J., & Capak, P. 2010, ApJ, 719, L50

Audard, M., Ábrahám, P., Dunham, M. M., et al. 2014, Protostars and Planets VI, 387

Bae, J., Hartmann, L., Zhu, Z., & Nelson, R. P. 2014, ApJ, 795, 61

Bae, J., Nelson, R. P., Hartmann, L., & Richard, S. 2016, ApJ, 829, 13

Bally, J., Devine, D., & Reipurth, B. 1996, ApJ, 473, L49

Bally, J., Lanber, W. D., Stark, A. A., & Wilson, R. W. 1987, ApJ, 312, L45

Bally, J., Walawender, J., Johnstone, D., Kirk, H., & Goodman, A. 2008, The Perseus Cloud, ed. B. Reipurth, 308

Balog, Z., Muzerolle, J., Flaherty, K., et al. 2014, ApJ, 789, L38

Baraffe, I., & Chabrier, G. 2010, A&A, 521, A44

Baraffe, I., Elbakyan, V. G., Vorobyov, E. I., & Chabrier, G. 2017, A&A, 597, A19

Barenfeld, S. A., Carpenter, J. M., Ricci, L., & Isella, A. 2016, ArXiv e-prints, arXiv:1605.05772

Bell, K. R., Lin, D. N. C., Hartmann, L. W., & Kenyon, S. J. 1995, ApJ, 444, 376

Berry, D. S. 2015, Astronomy and Computing, 10, 22

Billot, N., Morales-Calderón, M., Stauffer, J. R., Megeath, S. T., & Whitney, B. 2012, ApJ, 753, L35

Bonnell, I., & Bastien, P. 1992, ApJ, 401, L31

Bontemps, S., Andre, P., & Ward-Thompson, D. 1995, A&A, 297, 98

Bourke, T. L., Myers, P. C., Evans, II, N. J., et al. 2006, ApJ, 649, L37

Bower, G. C., Loinard, L., Dzib, S., et al. 2016, ApJ, 830, 107

Bower, G. C., Plambeck, R. L., Bolatto, A., et al. 2003, ApJ, 598, 1140

Buckle, J. V., Drabek-Maunder, E., Greaves, J., et al. 2015, MNRAS, 449, 2472

Caratti o Garatti, A., Garcia Lopez, R., Scholz, A., et al. 2011, A&A, 526, L1

Caratti O Garatti, A., Stecklum, B., Garcia Lopez, R., et al. 2016, Nature Physics, 13, 276

Casali, M. M., Eiroa, C., & Duncan, W. D. 1993, A&A, 275, 195

Chen, M. C.-Y., Di Francesco, J., Johnstone, D., et al. 2016, ApJ, 826, 95

Chini, R., Reipurth, B., Ward-Thompson, D., et al. 1997, ApJ, 474, L135

Choi, M., Kang, M., Byun, D.-Y., & Lee, J.-E. 2012, ApJ, 759, 136

Cieza, L., Williams, J., Kourkchi, E., et al. 2015, MNRAS, 454, 1909

Cieza, L. A., Casassus, S., Tobin, J., et al. 2016, ArXiv e-prints, arXiv:1607.03757

Cody, A. M., Hillenbrand, L. A., David, T. J., et al. 2017, ApJ, 836, 41

Cody, A. M., Stauffer, J., Baglin, A., et al. 2014, AJ, 147, 82

Contreras, Y., Rathborne, J., & Garay, G. 2013, MNRAS, 433, 251

Contreras Peña, C., Lucas, P. W., Minniti, D., et al. 2017, MNRAS, 465, 3011

Costigan, G., Vink, J. S., Scholz, A., Ray, T., & Testi, L. 2014, MNRAS, 440, 3444

Curtis, E. I., Richer, J. S., Swift, J. J., & Williams, J. P. 2010, MNRAS, 408, 1516

D'Angelo, C. R., & Spruit, H. C. 2010, MNRAS, 406, 1208

Davis, C. J., Matthews, H. E., Ray, T. P., Dent, W. R. F., & Richer, J. S. 1999, MNRAS, 309, 141

Dempsey, J. T., Friberg, P., Jenness, T., et al. 2013, MNRAS, 430, 2534

Dodds, P., Greaves, J. S., Scholz, A., et al. 2015, MNRAS, 447, 722

Duarte-Cabral, A., Fuller, G. A., Peretto, N., et al. 2010, A&A, 519, A27

Dunham, M. M., Crapsi, A., Evans, II, N. J., et al. 2008, ApJS, 179, 249

Dunham, M. M., Evans, II, N. J., Terebey, S., Dullemond, C. P., & Young, C. H. 2010, ApJ, 710, 470

Dunham, M. M., & Vorobyov, E. I. 2012, ApJ, 747, 52

Dunham, M. M., Stutz, A. M., Allen, L. E., et al. 2014, Protostars and Planets VI, 195

Dunham, M. M., Allen, L. E., Evans, II, N. J., et al. 2015, ApJS, 220, 11

Eiroa, C., Djupvik, A. A., & Casali, M. M. 2008, The Serpens Molecular Cloud, ed. B. Reipurth, 693

Elbakyan, V. G., Vorobyov, E. I., & Glebova, G. M. 2016, Astronomy Reports, 60, 879

Elias, J. H. 1978, ApJ, 224, 453

Enoch, M. L., Evans, II, N. J., Sargent, A. I., & Glenn, J. 2009, ApJ, 692, 973

Enoch, M. L., Glenn, J., Evans, II, N. J., et al. 2007, ApJ, 666, 982

Enoch, M. L., Young, K. E., Glenn, J., et al. 2006, ApJ, 638, 293

Fischer, W. J., Megeath, S. T., Tobin, J. J., et al. 2012, ApJ, 756, 99

Fischer, W. J., Megeath, S. T., Furlan, E., et al. 2017, ApJ, 840, 69

Forbrich, J., Reid, M. J., Menten, K. M., et al. 2017, ArXiv e-prints, arXiv:1706.05562

Forbrich, J., Rodríguez, L. F., Palau, A., et al. 2015, ApJ, 814, 15

Forgan, D., & Rice, K. 2010, MNRAS, 402, 1349

Friesen, R. K., Bourke, T. L., Di Francesco, J., Gutermuth, R., & Myers, P. C. 2016, ApJ, 833, 204

Friesen, R. K., Di Francesco, J., Shirley, Y. L., & Myers, P. C. 2009, ApJ, 697, 1457

Frimann, S., Jørgensen, J. K., Dunham, M. M., et al. 2017, ArXiv e-prints, arXiv:1703.10225

Gaia Collaboration, Brown, A. G. A., Vallenari, A., et al. 2016, ArXiv e-prints, arXiv:1609.04172

Gibb, A. G. 2008, Star Formation in NGC 2068, NGC 2071, and Northern L1630, ed. B. Reipurth, 693

Gibb, A. G., Jenness, T., & Economou, F. 2013, Starlink User Note, 265

Graves, S. F., Richer, J. S., Buckle, J. V., et al. 2010, MNRAS, 409, 1412

Green, J. D., Kraus, A. L., Rizzuto, A. C., et al. 2016, ApJ, 830, 29

Green, J. D., Evans, II, N. J., Kóspál, Á., et al. 2013, ApJ, 772, 117

Güdel, M. 2002, ARA&A, 40, 217

Gutermuth, R. A., Myers, P. C., Megeath, S. T., et al. 2008a, ApJ, 674, 336

Gutermuth, R. A., Bourke, T. L., Allen, L. E., et al. 2008b, ApJ, 673, L151

Hacar, A., Tafalla, M., & Alves, J. 2017, ArXiv e-prints, arXiv:1703.07029

Hacar, A., Tafalla, M., Kauffmann, J., & Kovács, A. 2013, A&A, 554, A55

Harsono, D., Bruderer, S., & van Dishoeck, E. F. 2015, A&A, 582, A41

Hartmann, L., Cassen, P., & Kenyon, S. J. 1997, ApJ, 475, 770

Hartmann, L., Herczeg, G., & Calvet, N. 2016, ARA&A, 54, 135

Hartmann, L., & Kenyon, S. J. 1985, ApJ, 299, 462

—. 1996, ARA&A, 34, 207

Harvey, P., Merín, B., Huard, T. L., et al. 2007, ApJ, 663, 1149

Hatchell, J., Richer, J. S., Fuller, G. A., et al. 2005, A&A, 440, 151

Hatchell, J., Wilson, T., Drabek, E., et al. 2013, MNRAS, 429, L10

Haubois, X., Dodds-Eden, K., Weiss, A., et al. 2012, A&A, 540, A41

Hennebelle, P., Lesur, G., & Fromang, S. 2017, A&A, 599, A86

Herbig, G. H. 1977, ApJ, 217, 693

—. 2008, AJ, 135, 637

Herbst, W. 2008, Star Formation in IC 348, ed. B. Reipurth, 372

Hillenbrand, L. A., & Findeisen, K. P. 2015, ApJ, 808, 68

Hillenbrand, L. A., Miller, A. A., Covey, K. R., et al. 2013, AJ, 145, 59

Hodapp, K. W. 1999, AJ, 118, 1338

Hodapp, K. W., & Chini, R. 2015, ApJ, 813, 107

Hodapp, K. W., Chini, R., Watermann, R., & Lemke, R. 2012, ApJ, 744, 56

Holland, W. S., Bintley, D., Chapin, E. L., et al. 2013, MNRAS, 430, 2513

Holoien, T. W.-S., Prieto, J. L., Stanek, K. Z., et al. 2014, ApJ, 785, L35

Hsieh, T.-H., Lai, S.-P., Belloche, A., & Wyrowski, F. 2016, ArXiv e-prints, arXiv:1605.03055

Hsieh, T.-H., Lai, S.-P., Belloche, A., Wyrowski, F., & Hung, C.-L. 2015, ApJ, 802, 126

Hunter, T. R., Brogan, C. L., MacLeod, G., et al. 2017, ArXiv e-prints, arXiv:1701.08637

Johnstone, D., & Bally, J. 1999, ApJ, 510, L49

Johnstone, D., Di Francesco, J., & Kirk, H. 2004, ApJ, 611, L45

Johnstone, D., Hendricks, B., Herczeg, G. J., & Bruderer, S. 2013, ApJ, 765, 133

Johnstone, D., Matthews, H., & Mitchell, G. F. 2006, ApJ, 639, 259

Johnstone, D., Wilson, C. D., Moriarty-Schieven, G., et al. 2000, ApJ, 545, 327

Jørgensen, J. K., Johnstone, D., Kirk, H., & Myers, P. C. 2007, ApJ, 656, 293

Jørgensen, J. K., Johnstone, D., Kirk, H., et al. 2008, ApJ, 683, 822

Jørgensen, J. K., Visser, R., Williams, J. P., & Bergin, E. A. 2015, A&A, 579, A23

Jørgensen, J. K., Visser, R., Sakai, N., et al. 2013, ApJ, 779, L22

Kaas, A. A., Olofsson, G., Bontemps, S., et al. 2004, A&A, 421, 623

Kackley, R., Scott, D., Chapin, E., & Friberg, P. 2010, in Proc. SPIE, Vol. 7740, Software and Cyberinfrastructure for Astronomy, 77401Z

Kamazaki, T., Saito, M., Hirano, N., & Kawabe, R. 2001, ApJ, 548, 278

Kastner, J. H., Richmond, M., Grosso, N., et al. 2006, ApJ, 648, L43

Kenyon, S. J., Hartmann, L. W., Strom, K. M., & Strom, S. E. 1990, AJ, 99, 869

Kern, N. S., Keown, J. A., Tobin, J. J., Mead, A., & Gutermuth, R. A. 2016, AJ, 151, 42

Kim, H. J., Evans, II, N. J., Dunham, M. M., Lee, J.-E., & Pontoppidan, K. M. 2012, ApJ, 758, 38

Kirk, H., Johnstone, D., & Di Francesco, J. 2006, ApJ, 646, 1009

Kirk, H., Myers, P. C., Bourke, T. L., et al. 2013, ApJ, 766, 115

Kirk, H., Johnstone, D., Di Francesco, J., et al. 2016, ApJ, 821, 98

Knee, L. B. G., & Sandell, G. 2000, A&A, 361, 671

Kóspál, Á., Ábrahám, P., Prusti, T., et al. 2007, A&A, 470, 211

Kóspál, Á., Salter, D. M., Hogerheijde, M. R., Moór, A., & Blake, G. A. 2011, A&A, 527, A96

Kóspál, Á., Ábrahám, P., Csengeri, T., et al. 2017, ApJ, 843, 45

Kounkel, M., Hartmann, L., Loinard, L., et al. 2017, ApJ, 834, 142

Kutner, M. L., Tucker, K. D., Chin, G., & Thaddeus, P. 1977, ApJ, 215, 521

Lada, E. A., Evans, II, N. J., & Falgarone, E. 1997, ApJ, 488, 286

Lane, J., Kirk, H., Johnstone, D., et al. 2016, ApJ, 833, 44

Larson, R. B. 1969, MNRAS, 145, 271

Lee, C. W., Kim, M.-R., Kim, G., et al. 2013, ApJ, 777, 50

Lee, C. W., Bourke, T. L., Myers, P. C., et al. 2009, ApJ, 693, 1290

Lee, K., Looney, L., Johnstone, D., & Tobin, J. 2012, ApJ, 761, 171

Lee, K. I., Fernández-López, M., Storm, S., et al. 2014, ApJ, 797, 76

Lin, D. N. C., Faulkner, J., & Papaloizou, J. 1985, MNRAS, 212, 105

Loinard, L., Torres, R. M., Mioduszewski, A. J., & Rodríguez, L. F. 2008, ApJ, 675, L29

Loren, R. B., & Wootten, A. 1986, ApJ, 306, 142

Loren, R. B., Wootten, A., & Wilking, B. A. 1990, ApJ, 365, 269

Luhman, K. L., Esplin, T. L., & Loutrel, N. P. 2016, ApJ, 827, 52

Machida, M. N., Inutsuka, S.-i., & Matsumoto, T. 2011, ApJ, 729, 42

Mairs, S., Johnstone, D., Kirk, H., et al. 2015, MNRAS, 454, 2557

Mairs, S., Lane, J., Johnstone, D., et al. 2017, ArXiv e-prints, arXiv:1706.01897

Massi, M., Forbrich, J., Menten, K. M., et al. 2006, A&A, 453, 959

Masunaga, H., & Inutsuka, S.-i. 2000, ApJ, 531, 350

Maury, A. J., André, P., Men'shchikov, A., Könyves, V., & Bontemps, S. 2011, A&A, 535, A77

Megeath, S. T., Gutermuth, R., Muzerolle, J., et al. 2012, AJ, 144, 192

—. 2016, AJ, 151, 5

Meyer, M. R., Flaherty, K., Levine, J. L., et al. 2008, Star Formation in NGC 2023, NGC 2024, and Southern L1630, ed. B. Reipurth, 662

Mezger, P. G., Zylka, R., & Wink, J. E. 1990, A&A, 228, 95

Miller, A. A., Hillenbrand, L. A., Covey, K. R., et al. 2011, ApJ, 730, 80

Motte, F., André, P., & Neri, R. 1998, A&A, 336, 150

Muñoz, D. J., & Lai, D. 2016, ApJ, 827, 43

Muzerolle, J., Furlan, E., Flaherty, K., Balog, Z., & Gutermuth, R. 2013, Nature, 493, 378

Myers, P. C. 2012, ApJ, 752, 9

Nakamura, F., Takakuwa, S., & Kawabe, R. 2012, ApJ, 758, L25

Nutter, D., & Ward-Thompson, D. 2007, MNRAS, 374, 1413

Offner, S. S. R., & McKee, C. F. 2011, ApJ, 736, 53

Olmi, L., & Testi, L. 2002, A&A, 392, 1053

Onozato, H., Ita, Y., Ono, K., et al. 2015, PASJ, 67, 39

Ortiz-León, G. N., Loinard, L., Kounkel, M. A., et al. 2017a, ApJ, 834, 141

Ortiz-León, G. N., Dzib, S. A., Kounkel, M. A., et al. 2017b, ApJ, 834, 143

Owen, J. E., & Jacquet, E. 2015, MNRAS, 446, 3285

Pan, Z., Li, D., Chang, Q., et al. 2017, ApJ, 836, 194

Panopoulou, G. V., Psaradaki, I., Skalidis, R., Tassis, K., & Andrews, J. J. 2017, MNRAS, 466, 2529

Pascucci, I., Testi, L., Herczeg, G. J., et al. 2016, ArXiv e-prints, arXiv:1608.03621

Pattle, K., Ward-Thompson, D., Kirk, J. M., et al. 2015, MNRAS, 450, 1094

—. 2017, MNRAS, 464, 4255

Peterson, D. E., Megeath, S. T., Luhman, K. L., et al. 2008, ApJ, 685, 313

Plunkett, A. L., Arce, H. G., Mardones, D., et al. 2015, Nature, 527, 70

Pon, A., Plume, R., Friesen, R. K., et al. 2009, ApJ, 698, 1914

Raga, A. C., de Gouveia Dal Pino, E. M., Noriega-Crespo, A., Mininni, P. D., & Velázquez, P. F. 2002, A&A, 392, 267

Rebull, L. M., Cody, A. M., Covey, K. R., et al. 2014, AJ, 148, 92

Reipurth, B. 1989, Nature, 340, 42

Reipurth, B., & Aspin, C. 2004, ApJ, 606, L119

Romanova, M. M., Ustyugova, G. V., Koldoba, A. V., & Lovelace, R. V. E. 2013, MNRAS, 430, 699

Sadavoy, S. I., Di Francesco, J., Bontemps, S., et al. 2010, ApJ, 710, 1247

Safron, E. J., Fischer, W. J., Megeath, S. T., et al. 2015, ApJ, 800, L5

Salji, C. J., Richer, J. S., Buckle, J. V., et al. 2015, MNRAS, 449, 1782

Salter, D. M., Kóspál, Á., Getman, K. V., et al. 2010, A&A, 521, A32

Scholz, A., Froebrich, D., & Wood, K. 2013a, MNRAS, 430, 2910

Scholz, A., Geers, V., Clark, P., Jayawardhana, R., & Muzic, K. 2013b, ApJ, 775, 138

Scholz, A., Jayawardhana, R., Muzic, K., et al. 2012a, ApJ, 756, 24

Scholz, A., Muzic, K., Geers, V., et al. 2012b, ApJ, 744, 6

Shu, F. H. 1977, ApJ, 214, 488

Shu, F. H., Adams, F. C., & Lizano, S. 1987, ARA&A, 25, 23

Skinner, S., Gagné, M., & Belzer, E. 2003, ApJ, 598, 375

Spezzi, L., Petr-Gotzens, M. G., Alcalá, J. M., et al. 2015, A&A, 581, A140

Stamatellos, D., Whitworth, A. P., & Hubber, D. A. 2011, ApJ, 730, 32

—. 2012, MNRAS, 427, 1182

Stanke, T., Smith, M. D., Gredel, R., & Khanzadyan, T. 2006, A&A, 447, 609

Strom, S. E., Vrba, F. J., & Strom, K. M. 1976, AJ, 81, 638

Stutz, A. M., Tobin, J. J., Stanke, T., et al. 2013, ApJ, 767, 36

Takahashi, S., Ho, P. T. P., Teixeira, P. S., Zapata, L. A., & Su, Y.-N. 2013, ApJ, 763, 57

Takahashi, S., Saigo, K., Ho, P. T. P., & Tomida, K. 2012, ApJ, 752, 10

Takahashi, S., Saito, M., Ohashi, N., et al. 2008, ApJ, 688, 344

Tetarenko, A. J., Sivakoff, G. R., Miller-Jones, J. C. A., et al. 2017, MNRAS, 469, 3141

Thronson, Jr., H. A., Lada, C. J., Schwartz, P. R., et al. 1984, ApJ, 280, 154

Tobin, J. J., Hartmann, L., Chiang, H.-F., et al. 2011, ApJ, 740, 45

Tobin, J. J., Stutz, A. M., Megeath, S. T., et al. 2015, ApJ, 798, 128

Tsujimoto, M., Koyama, K., Tsuboi, Y., Goto, M., & Kobayashi, N. 2002, ApJ, 566, 974

van Leeuwen, F. 2007, A&A, 474, 653

Venuti, L., Bouvier, J., Flaccomio, E., et al. 2014, A&A, 570, A82

Visser, A. E., Richer, J. S., Chandler, C. J., & Padman, R. 1998, MNRAS, 301, 585

Visser, R., Bergin, E. A., & Jørgensen, J. K. 2015, A&A, 577, A102

Vorobyov, E., Elbakyan, V., Hosokawa, T., et al. 2017a, ArXiv e-prints, arXiv:1706.00502

Vorobyov, E. I., Baraffe, I., Harries, T., & Chabrier, G. 2013, A&A, 557, A35

Vorobyov, E. I., & Basu, S. 2005, ApJ, 633, L137

—. 2010, ApJ, 719, 1896

—. 2015, ApJ, 805, 115

Vorobyov, E. I., Elbakyan, V., Dunham, M. M., & Guedel, M. 2017b, A&A, 600, A36

Vorobyov, E. I., Pavlyuchenkov, Y. N., & Trinkl, P. 2014, Astronomy Reports, 58, 522

Vrba, F. J. 1977, AJ, 82, 198

Walawender, J., Bally, J., Francesco, J. D., Jørgensen, J., & Getman, K. . 2008, NGC 1333: A Nearby Burst of Star Formation, ed. B. Reipurth, 346

Walawender, J., Bally, J., Kirk, H., et al. 2006, AJ, 132, 467

Ward-Thompson, D., Di Francesco, J., Hatchell, J., et al. 2007, PASP, 119, 855

White, G. J., Drabek-Maunder, E., Rosolowsky, E., et al. 2015, MNRAS, 447, 1996

Wilking, B. A., Gagné, M., & Allen, L. E. 2008, in Handbook of Star Forming Regions, Volume II, ed. B. Reipurth, 351

Williams, J. P., Plambeck, R. L., & Heyer, M. H. 2003, ApJ, 591, 1025

Williams, J. P., Cieza, L. A., Andrews, S. M., et al. 2013, MNRAS, 435, 1671

Yan, J., Wang, H., Wang, M., et al. 1998, AJ, 116, 2438

Young, C. H., Jørgensen, J. K., Shirley, Y. L., et al. 2004, ApJS, 154, 396

Young, K. E., Enoch, M. L., Evans, II, N. J., et al. 2006, ApJ, 644, 326

Zhu, Z., Hartmann, L., Calvet, N., et al. 2008, ApJ, 684, 1281

Zhu, Z., Hartmann, L., Gammie, C., & McKinney, J. C. 2009, ApJ, 701, 620

Zhu, Z., Hartmann, L., Gammie, C. F., et al. 2010, ApJ, 713, 1134

APPENDIX

Table 2 lists the 850 μm peak flux per beam for bright (> 125 mJy/beam) sources associated with protostars. To be associated with a protostar, the peak flux location of the emission source must be less than 7″ from the protostar position previously listed in the *Spitzer*/IRS and MIPS mid-IR photometric catalogues of Dunham et al. (2015) and Megeath et al. (2016). The emission sources are identified using the JCMT Science Archive algorithm JSA_catalogue found in Starlinks PICARD package (Gibb et al. 2013), which uses the FELLWALKER routine (for more information, see Berry 2015). The peaks are then numbered in order of brightness. Table 2 lists the 102 protostars or disks that are associated with 93 distinct bright peaks. In some cases, more than one protostar is located near a single 850 μm peak, and in one case a peak is associated with both a protostar and a disk (counted as a protostar in the numbers presented in the main text). Some associations between peaks and disks and protostars may be coincidental.

TABLE 2
Protostars and disks identified with bright sub-mm peaks[a]

Region	ID	Peak[a]	Dist. (″)[b]	Name[c]	Region	ID	Peak[a]	Dist. (″)[b]	Name[c]
		Protostars					Protostars		
NGC 1333	1	9.43	0.37	J032910.4+311331	Oph Core	15	0.35	2.43	J162726.9-244050
NGC 1333	2	3.95	1.92	J032912.0+311305	Oph Core	20	0.27	5.0	J162709.4-243718
NGC 1333	2	3.95	5.92	J032912.0+311301	Oph Core	24	0.25	6.19	J162640.4-242714
NGC 1333	3	2.88	6.66	J032903.7+311603	Oph Core	25	0.25	5.89	J162623.5-242439
NGC 1333	4	2.45	2.67	J032855.5+311436	Oph Core	27	0.23	1.03	J162821.6-243623
NGC 1333	5	1.12	3.09	J032910.9+311826	Oph Core	28	0.22	5.89	J162727.9-243933
NGC 1333	5	1.12	3.39	J032911.2+311831	Oph Core	29	0.21	3.22	J162644.1-243448
NGC 1333	9	0.59	3.63	J032913.5+311358	Oph Core	32	0.19	3.84	J162705.2-243629
NGC 1333	11	0.47	2.03	J032857.3+311415	Oph Core	37	0.15	2.93	J162739.8-244315
NGC 1333	12	0.46	2.27	J032837.0+311330	Oph Core	39	0.15	5.01	J162617.2-242345
NGC 1333	13	0.44	3.07	J032904.0+311446	Serpens Main	1	6.76	3.16	J182949.6+011521
NGC 1333	17	0.37	2.1	J032900.5+311200	Serpens Main	3	2.12	1.5	J182948.1+011644
NGC 1333	21	0.32	1.45	J032917.1+312746	Serpens Main	4	1.78	2.0	J182959.2+011401
NGC 1333	21	0.32	4.25	J032917.5+312748	Serpens Main	5	1.16	6.7	J183000.7+011301
NGC 1333	22	0.32	2.56	J032907.7+312157	Serpens Main	7	1.06	2.5	J182951.1+011640
NGC 1333	24	0.27	6.63	J032840.6+311756	Serpens Main	8	0.85	1.53	J182957.7+011405
NGC 1333	28	0.23	1.78	J032834.5+310705	Serpens Main	9	0.81	4.23	J182952.2+011547
IC 348	1	1.42	2.16	J034356.5+320052	Serpens Main	15	0.28	2.54	J182931.9+011842
IC 348	2	1.16	2.68	J034356.8+320304	Serpens South	10	0.66	5.56	J182938.1-015100
IC 348	3	0.57	2.64	J034443.9+320136	Serpens South	17	0.45	3.0	J183025.8-021042
IC 348	3	0.57	6.51	J034443.3+320131	Serpens South	25	0.3	6.7	J182959.4-020106
IC 348	4	0.34	1.27	J034350.9+320324	Serpens South	31	0.2	4.0	J183001.0-020608
IC 348	9	0.15	1.14	J034412.9+320135	Serpens South	32	0.2	5.74	J183017.4-020958
OMC 2/3	2	5.96	6.53	2293	Serpens South	32	0.2	5.91	J183017.0-020958
OMC 2/3	3	5.6	3.08	2433	Serpens South	34	0.2	6.46	J183015.6-020719
OMC 2/3	6	2.66	5.8	2302	Serpens South	40	0.16	6.0	J182947.0-015548
OMC 2/3	7	2.54	3.24	2437	Serpens South	42	0.16	3.98	J182912.8-020350
OMC 2/3	13	1.74	3.53	2369	Serpens South	43	0.16	2.62	J182943.9-021255
OMC 2/3	13	1.74	6.85	2366	Serpens South	45	0.15	1.66	J182943.3-015651
OMC 2/3	17	1.58	3.51	2407					
OMC 2/3	18	1.46	1.94	2323			Disks		
OMC 2/3	20	1.39	1.25	2254	NGC 1333	32	0.16	5.88	J032856.1+311908
OMC 2/3	21	1.34	4.93	2469	OMC 2/3	5	3.62	2.94	2072
OMC 2/3	22	1.25	3.91	2187	OMC 2/3	15	1.63	6.6	2334
OMC 2/3	76	0.26	5.2	2456	OMC 2/3	19	1.45	3.98	2029
OMC 2/3	86	0.22	2.6	2510	OMC 2/3	25	1.06	4.84	2345
NGC 2068	1	2.54	3.79	3166	OMC 2/3	29	0.78	6.67	2371
NGC 2068	5	1.02	5.12	3201	OMC 2/3	47	0.45	1.07	2179
NGC 2068	5	1.02	5.78	3202	OMC 2/3	51	0.41	1.99	2347
NGC 2068	6	0.62	5.72	3168	OMC 2/3	61	0.32	3.8	2184
NGC 2068	6	0.62	5.76	3167	OMC 2/3	72	0.28	6.81	2145
NGC 2068	7	0.59	4.92	3203	OMC 2/3	75	0.26	5.35	2333
NGC 2068	8	0.57	2.94	3211	OMC 2/3	83	0.23	4.72	2363
NGC 2068	11	0.52	2.25	3159	OMC 2/3	101	0.19	6.31	2228
NGC 2068	13	0.44	6.25	3215	NGC 2024	30	0.17	3.33	2927
NGC 2068	22	0.29	0.83	3160	Oph Core	4	0.66	6.25	J162624.0-241613
NGC 2068	24	0.29	1.16	3180	Oph Core	6	0.59	4.36	J162645.0-242307
NGC 2024	4	5.94	3.37	2955	Oph Core	8	0.47	6.24	J162323.6-244314
NGC 2024	6	0.82	6.71	2867	Oph Core	18	0.28	4.89	J162610.3-242054
NGC 2024	26	0.19	4.02	3085	Oph Core	36	0.17	2.96	J162816.5-243657
Oph Core	2	3.98	5.3	J162626.4-242430	Oph Core	40	0.14	2.99	J162715.8-243843
Oph Core	13	0.39	3.71	J162730.1-242743	Serpens South	31	0.2	5.41	J183001.3-020609

[a] Jy beam^{-1}

[b] Distance between centroid of sub-mm peak and mid-IR position

[c] Dunham et al. (2015) and Megeath et al. (2016).